

Article

Nature of Ore Fluid at the Sopokomil Zn-Pb Deposit, North Sumatra, Indonesia: Implications for Metal Transport and Sulfide Deposition

Tomy Alvin Rivai ^{1,2,*} , Syafrizal ³ , Kotaro Yonezu ², Kenzo Sanematsu ¹ and Koichiro Watanabe ²

¹ Geological Survey of Japan, National Institute of Advanced Industrial Science and Technology, Central-7 1-1-1 Higashi, Tsukuba 305-8567, Japan; k-sanematsu@aist.go.jp

² Department of Earth Resources Engineering, Faculty of Engineering, Kyushu University, 744 Motoooka, Nishiku, Fukuoka 819-0395, Japan; yone@mine.kyushu-u.ac.jp (K.Y.); wat@mine.kyushu-u.ac.jp (K.W.)

³ Earth Resources Exploration Research Group, Faculty of Mining and Petroleum Engineering, Bandung Institute of Technology, Ganesha 10, Bandung 40132, Indonesia; syafrizal@mining.itb.ac.id

* Correspondence: tomy.rivai@aist.go.jp

Abstract: Little is known about the nature of ore fluid at the Sopokomil shale-hosted massive sulfide Zn-Pb deposit (North Sumatra, Indonesia). We therefore investigated its ore-fluid salinities, temperatures, densities, redox state, and pH using fluid inclusion microthermometry, sphalerite composition, and thermodynamic modelling. The fluid salinities and temperatures were ≈ 6 wt.% NaCl equiv and ≈ 165 °C, respectively, corresponding to an ore fluid less dense than seawater (≈ 0.96 g/mL). Sphalerite contains ≈ 9.9 mole% FeS in the stratiform ore and ≈ 3.4 mole% FeS in the feeder ore, suggesting a reduced fluid, which must have been acidic to be fertile. Such redox state and acidity invoke fluid dilution as the sulfide depositional mechanism. The bulk of the sulfides were precipitated in the early stage of mixing, within $T = 165$ – 155 °C. Key ingredients of sphalerite and galena at Sopokomil include (1) Zn that was primarily transported as $ZnCl^+$, (2) Pb that predominantly occurred as $PbCl_2(aq)$, and (3) S that was largely supplied by marine sediment porewater. This study highlights the significance of a dramatic shift in thermal and chemical equilibrium induced by fluid dilution in the making of the first significant shale-hosted massive sulfide Zn-Pb deposit in Indonesia.

Keywords: SEDEX; sedimentary exhalative; Dairi; Southeast Asia resources; sediment-hosted Zn-Pb; massive sulfides; base metals; stratiform Zn-Pb; SHMS



Citation: Rivai, T.A.; S.; Yonezu, K.; Sanematsu, K.; Watanabe, K. Nature of Ore Fluid at the Sopokomil Zn-Pb Deposit, North Sumatra, Indonesia: Implications for Metal Transport and Sulfide Deposition. *Geosciences* **2021**, *11*, 298. <https://doi.org/10.3390/geosciences11070298>

Academic Editor: Patrick Seyler

Received: 4 June 2021

Accepted: 17 July 2021

Published: 19 July 2021

Publisher's Note: MDPI stays neutral with regard to jurisdictional claims in published maps and institutional affiliations.



Copyright: © 2021 by the authors. Licensee MDPI, Basel, Switzerland. This article is an open access article distributed under the terms and conditions of the Creative Commons Attribution (CC BY) license (<https://creativecommons.org/licenses/by/4.0/>).

1. Introduction

The Sopokomil Zn-Pb deposit is thus far the only major shale-hosted massive sulfide (SHMS) deposit discovered on Sumatra, Indonesia (Figure 1A), hosting 25.1 Mt of ore resources at 10.1 wt.% Zn and 6.0 wt.% Pb [1]. Its hosted metal resources (4 Mt Zn + Pb) make Sopokomil one of the most significant SHMS deposits on Earth [2]. Apart from Sopokomil, all known Zn-Pb resources on Sumatra occur as skarn-, vein-, and MVT-type deposits [3–5]. On account of its economically attractive metal content and the regional scarcity of SHMS deposits, Sopokomil offers an ideal opportunity to improve our current understanding on Zn-Pb metallogenesis on the island. Despite this, only a few studies have been hitherto carried out [6–8]. Thus, some of the deposit aspects, including the nature of its ore fluid [9–11], are still poorly constrained.

Based on ore-fluid chemistry, there are two key depositional mechanisms that dominate in the formation of SHMS deposits: fluid dilution and steep redox gradient [12]. The first mechanism invokes the cooling and neutralization of a reduced, acidic ore fluid [13,14]. The second mechanism forces an oxidized, near-neutral ore fluid to drop its metal content due to interaction with reduced strata in the SHMS-hosting basin [12,15]. Thus, under-

standing the nature of ore fluid can give us insights into the depositional mechanism at Sopokomil.

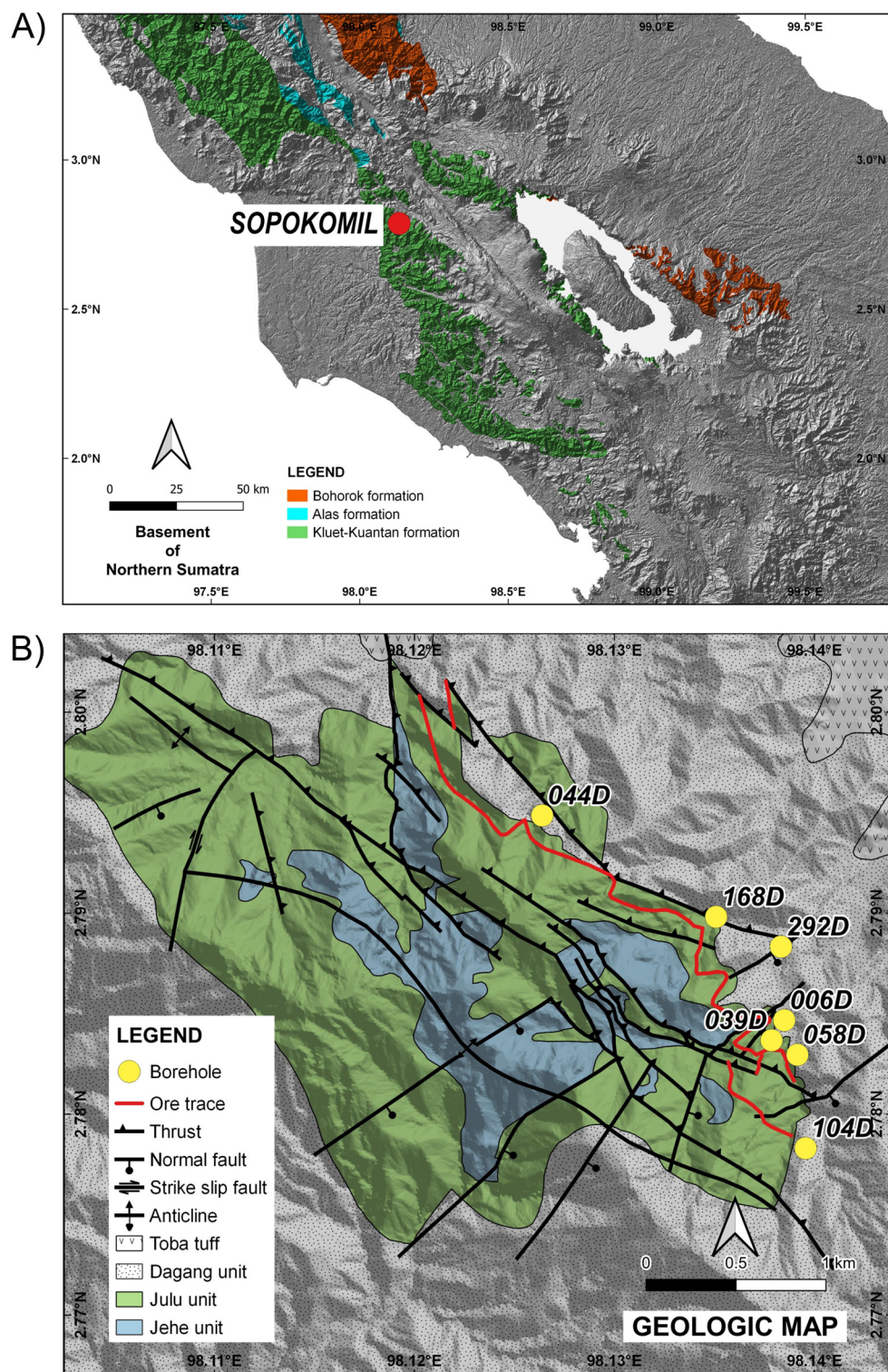


Figure 1. (A) Distribution of North Sumatra basement rocks (modified after [16–18]). Location of the Sopokomil deposit is indicated by closed, red circle. (B) Geologic map of the Sopokomil deposit. Borehole collars from which the samples in this study were collected are marked by closed, yellow circles.

The objective of this study is to comprehend the nature of the Sopokomil ore fluid and its implications to metal transport and sulfide deposition. The required parameters include fluid temperatures, salinities, densities, redox state, and pH. The depositional temperatures and salinities are estimated using fluid inclusion microthermometry. They are then used to infer the ore-fluid densities. The microthermometry data, coupled with sphalerite compositional data, are utilized to deduce the redox state and pH. Complemented by the concept of dual S-sources [7], all these fluid parameters are subsequently discussed in connection with transport chemistry and depositional mechanisms leading to the formation of the Sopokomil SHMS Zn-Pb deposit.

2. Geologic Background

2.1. Regional and Local Geology

North Sumatra basement is made up of the Bohorok, Alas, and Kluet-Kuantan formations [19]. The Late Carboniferous-Early Permian Bohorok Formation is marked by the presence of diamictite, indicating a glacio-marine depositional environment [20]. The Early Carboniferous Alas Formation consists mainly of limestone hosting fossils of temperate environment origin [21]. The Bohorok and Alas formations are the basement of the Sibumasu Block. The Kluet-Kuantan Formation, in which the Sopokomil deposit is hosted (Figure 1A), is the basement of the West Sumatra Block. It comprises quartzwacke, sandstone, and shale intercalated by limestone lenses and was deposited in the tropical environment during the Early Carboniferous [21], a period during which the block was a part of the Indochina Terrane. The North Sumatra basement was subjected to regional, sub-greenschist to greenschist metamorphism as indicated by widespread slate and phyllite [22].

Rocks in the vicinity of the Sopokomil deposit are grouped into three units. From top downward, they are the Dagang, Julu, and Jehe units (Figure 1B). The Dagang unit consists of interbedded dolomitic sandstone and siltstone with minor black shale deposited in a carbonate platform. Transition to the underlying Julu unit is gradational. The Julu unit is composed of interbedded black shale and dolomitic siltstone. It has a sharp contact with the underlying arenaceous massive and brecciated dolostone in the Jehe unit, inferring a rapid transgressive event.

2.2. Mineralization

Ores at Sopokomil extend along the NE limb of the NW-SE anticline and are hosted in the Julu and Jehe units (Figure 1B). The Julu unit hosts multi-horizon, stratiform ore (lower, main, and upper ore horizons) with thickness up to 20 m in the SE portion and up to 5 m in the NW portion. The Jehe unit hosts discordant feeder mineralization. However, having a tenor smaller and less continued than its stratiform counterpart, the feeder ore is of lesser economic significance.

The stratiform ore is divided into pyrite-rich massive, sphalerite-rich massive, banded sulfide, galena-rich breccia, and vein ore-types, whereas the feeder mineralization comprises vein and replacement ore-types [7]. Both ores contain sphalerite and galena as principal ore minerals, with quartz, dolomite, minor Ba-bearing K-feldspar, and locally present trace barite and calcite as gangue minerals. Iron sulfide phases consist of pyrite and pyrrhotite, although the latter is confined to the lower ore horizon. Accessory ore minerals in the stratiform ore comprise tetrahedrite, bournonite, and chalcopyrite, while those in the feeder mineralization consist of tetrahedrite, chalcopyrite, tennantite, arsenopyrite, pyrrhotite, acanthite, freieslebenite, boulangerite, and diaphorite. Tetrahedrite and chalcopyrite in the feeder ore are more abundant than those in the stratiform ore (Figure 2).

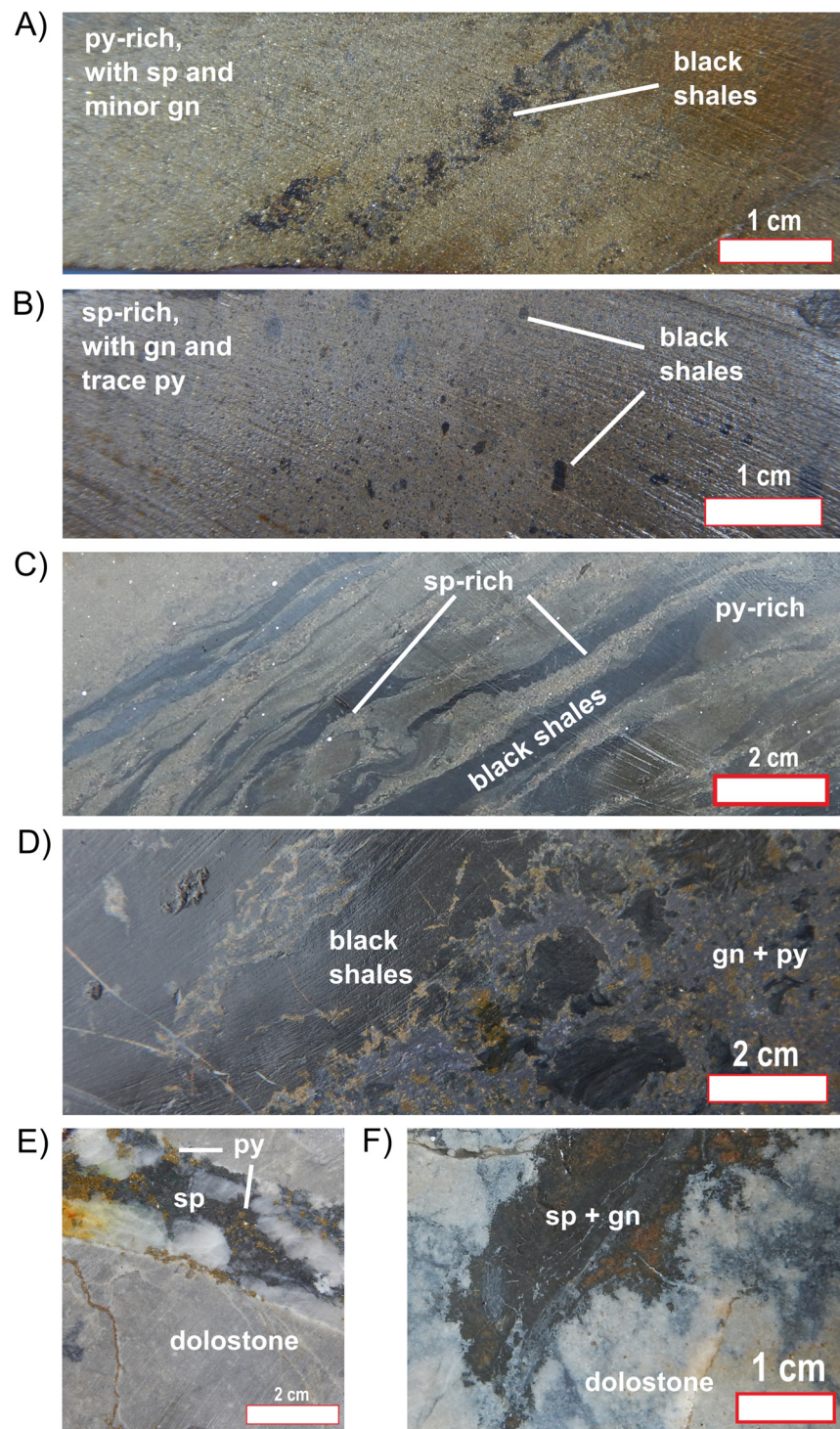


Figure 2. Ore types at the Sopokomil deposit confirming their textural classification by [7]: (A) pyrite-rich massive, (B) sphalerite-rich massive, (C) banded sulfide, (D) galena-rich breccia, (E) vein, and (F) replacement ore-types.

The concept of dual S-sources was introduced to explain the S-isotope ratio in the Sopokomil sulfides [7]. In the barren sedimentary rocks, the S-isotope ratio ($\delta^{34}\text{S} = -4.1$ to $+9.7\%$) suggest that bacterial sulfate reduction (BSR) operated in the Sopokomil Basin. As mineralization took place, the BSR produced much heavier sulfides: (1) $\delta^{34}\text{S} = +6.4$ to $+18.1\%$ in the lower ore horizon, (2) $\delta^{34}\text{S} = +13.5$ to $+28.8\%$ in the main ore horizon, and (3) $\delta^{34}\text{S} = +18.7$ to $+26.7\%$ in the upper ore horizon. Conversely, sulfides in the Jehe unit

are distinctively light ($\delta^{34}\text{S} = +3.5$ to $+8.0\%$), pointing out a contribution of hydrothermal S to the feeder mineralization. Considering that the economic mineralization is limited to the stratiform ore, reduced S of bacteriogenic origin is thought to be responsible for the growth of the Sopokomil deposit [7].

3. Methods

3.1. Ore Mineralogy

To investigate ore mineralogy of the samples, standard polished sections were prepared. They were analyzed under reflected light using a polarizing microscope Nikon ECLIPSE LV100POL at Kyushu University and a polarizing microscope Nikon ECLIPSE E600POL at Geological Survey of Japan.

3.2. Fluid Inclusion Microthermometry

Fluid inclusion (FI) wafers were prepared from sphalerite-bearing samples. They were examined under a polarizing microscope Nikon ECLIPSE LV100POL prior to freezing and heating experiments. The FI microthermometry was carried out using a LINKAM stage THMS600, routinely calibrated by nonane, decane, dodecane, tridecane, dodecanediol, benzanilide, and sodium nitrate. During the stage operation, the lowest temperature set in the freezing experiment was $-60\text{ }^\circ\text{C}$. The stage was then heated with an increment rate of $20\text{ }^\circ\text{C}/\text{min}$ that was sequentially reduced to $0.1\text{ }^\circ\text{C}/\text{min}$ as the stage temperature became closer to final ice melting (T_m) and homogenization temperatures (T_h). The FI analysis was conducted at Kyushu University, Japan.

3.3. Density Modeling

Ore-fluid densities were modelled using the equation of [23]. The model calculated evolving densities as the ore fluid was continuously diluted by marine sediment porewater. Temperatures and salinities of the ore fluid were taken from the results of FI microthermometry and those of sediment porewater were assumed to be 3.5 wt.% NaCl equiv and $3\text{ }^\circ\text{C}$, respectively.

3.4. EPMA

Sphalerite composition in the stratiform and feeder ores was quantified using a Field Emission Electron Probe Micro Analyzer (EPMA) JEOL JXA-8530F at Geological Survey of Japan. The quantitative analysis was performed at an accelerating voltage of 20 kV and a probe current of 20 nA, with JEOL standards of ZnS for Zn, FeS₂ for Fe and S, copper for Cu, CdS for Cd, InAs for In, and GaSb for Ga as reference materials. X-ray intensity of ZnK α , FeK α , SK α , CuK α , CdL α , InL α , and GaL α was measured in 20 s at the peak and in 10 s at the background. The sphalerite composition was then calculated based on the atomic per formula unit (apfu) method and was used to estimate redox state of the ore fluid.

3.5. Thermodynamic Modelling

Ore-fluid pH, Zn-Pb transport chemistry, and sulfides depositional mechanism were evaluated through thermodynamic modelling. The modelling was carried out in GEM-selektor version 3, utilizing SUPCRT thermodynamic database [24–27]. Ion-association with extended Debye–Hueckel equation and ideal mixture of gaseous components were selected as the aqueous electrolyte and gas-fluid mixture models, respectively. Solid phases were controlled by sphalerite, galena, pyrite, pyrrhotite, calcite, and dolomite.

The ore-fluid pH was calculated at different ΣZn and ΣPb ranging from 1 to 100 ppm, values considered as their fertility windows in SHMS ore fluids and as their general concentrations in basinal fluids [12,28,29]. The $\Sigma\text{Zn}/\Sigma\text{Pb}$ ratio was fixed at 2, given the ratio of Zn and Pb grades in the Sopokomil ores [1]. Other fluid constraints were $\Sigma\text{Fe} = 10^{-3}$ molal (m), $\Sigma\text{S} = 10^{-3} m$, $\Sigma\text{C} = 0.256 m$, and $\Sigma\text{Na}:\Sigma\text{K}:\Sigma\text{Ca}$ following [12]. Temperatures and salinities were constrained by the results of FI microthermometry. In each run, 0.0001 m HCl was sequentially added until no galena or sphalerite precipitated.

The Zn-Pb transportation and sulfide deposition were modelled by adding marine sediment porewater to 1 kg of ore fluid. The ore-fluid composition was constrained by $\Sigma\text{Fe} = 10^{-3} m$, $\Sigma\text{S} = 10^{-3} m$, $\Sigma\text{C} = 0.256 m$, $\Sigma\text{Zn} = 100 \text{ ppm}$, $\Sigma\text{Pb} = 50 \text{ ppm}$, pH resulting from the ore-fluid pH simulation, and $\Sigma\text{Na}:\Sigma\text{K}:\Sigma\text{Ca}$ following [12] (Table A1 in Appendix A). Temperatures and salinities were constrained by the results of FI microthermometry. The composition of marine sediment porewater was assumed to be close to that of seawater, with values referred to [30] (Table A1). Temperatures and salinities of marine sediment porewater were 3 °C and 3.5 wt.% NaCl equiv, respectively. The mass of aqueous phase generated in each run was used as the mass of ore fluid in the subsequent calculation. Sediment porewater/ore fluid ratio sequentially increased from 0 to 0.1, with an increment rate of 0.01/run. The calculations were conducted at equilibrium temperatures and $P = 250 \text{ bars}$ [14].

4. Results

4.1. Sample Mineralogy

Samples from the stratiform ore represent pyrite-rich massive and sphalerite-rich massive ore-types. In the first ore-type, ore mineralogy was dominated by cubic pyrite and sphalerite. Sphalerite occurred in the interstitial spaces of pyrite, intergrown by minor galena and gangue minerals (Figure 3A). In the second ore-type, sphalerite was intergrown by minor galena (Figure 3B), locally by pyrrhotite as well (Figure 3C). Chalcopyrite and pyrite were present in trace amounts. Black shale lenses and fragments were frequently observed in this ore-type. They aligned in a parallel manner to the sedimentary bedding (Figure 3D).

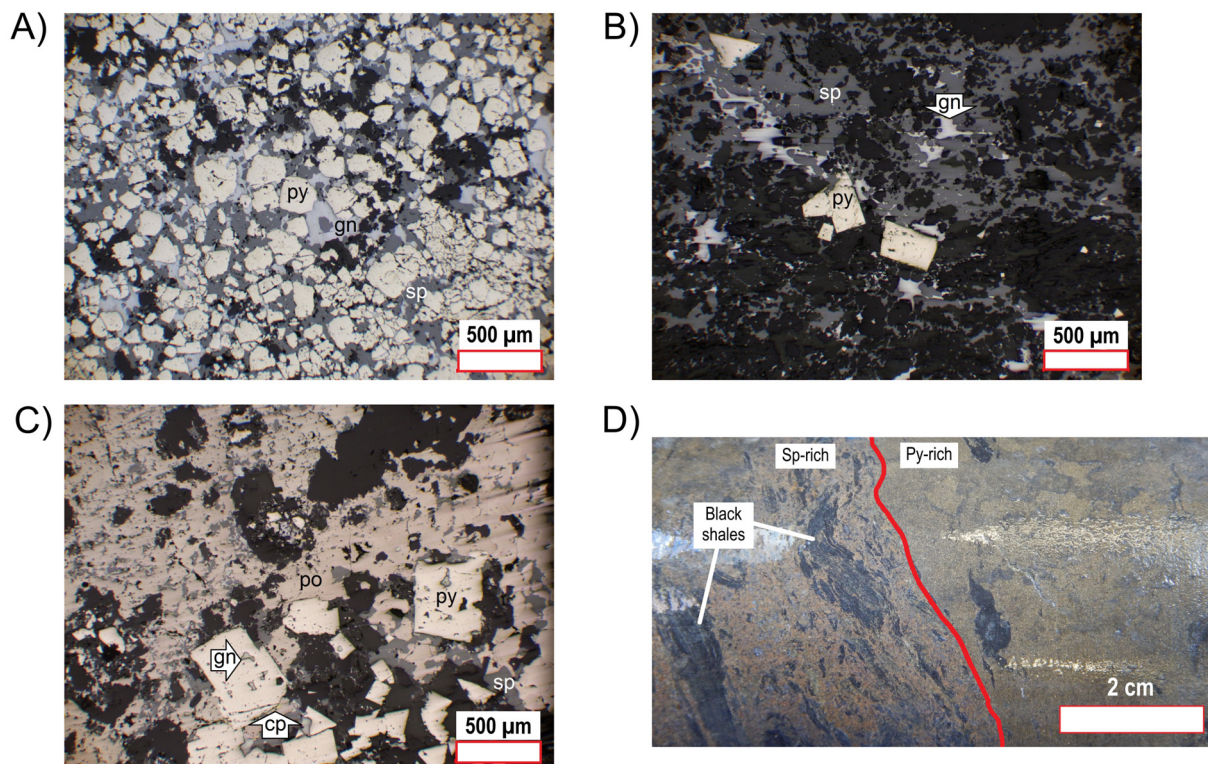


Figure 3. Cont.

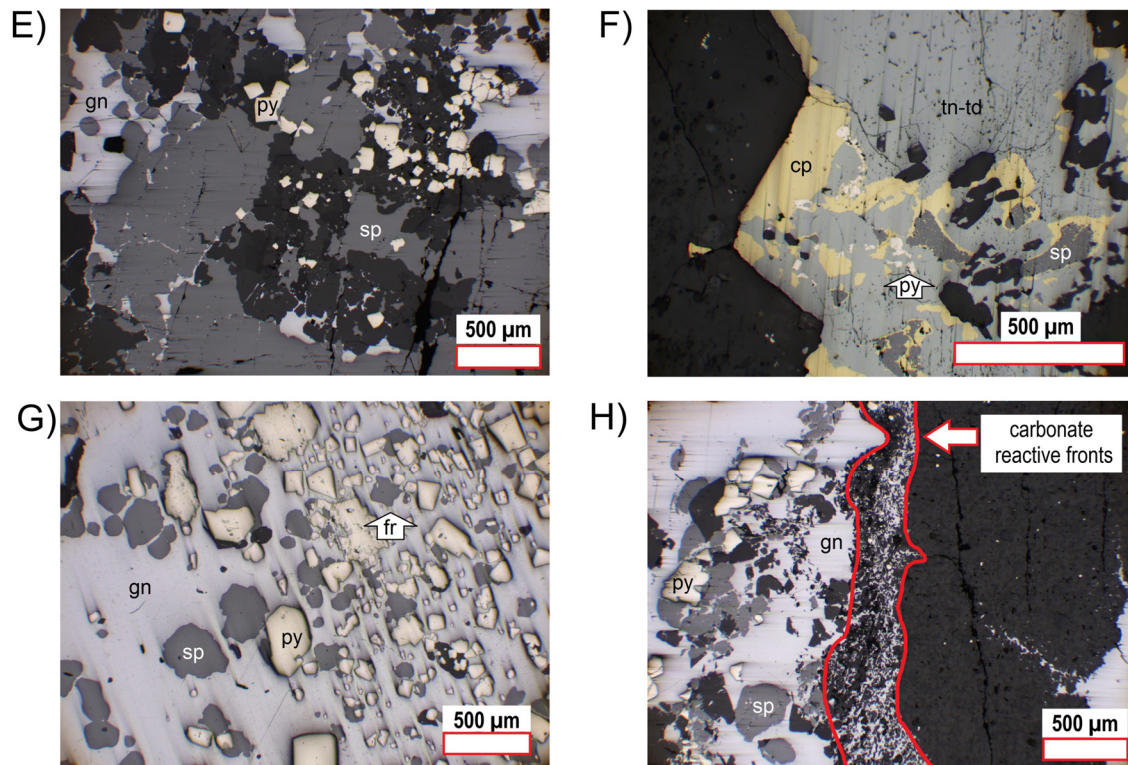


Figure 3. (A) Sphalerite intergrown by galena and gangues in the interstitial spaces of pyrite in pyrite-rich massive ore-type. (B) Sphalerite intergrown by minor galena in sphalerite-rich massive ore-type. (C) Sphalerite intergrown by pyrrhotite in sphalerite-rich massive ore-type. (D) Black shale fragments and lenses within ore, parallel to sedimentary bedding. (E) Sphalerite, galena, and pyrite in vein ore-type. (F) Vein ore-type rich in Ag-sulfosalts and chalcopyrite. (G) Occurrence of Pb-Ag-Cu sulfosalts in replacement ore-type. (H) Boundary between replaced and unreplaced carbonate rocks. Abbreviations: cp (chalcopyrite), fr (freieslebenite), gn (galena), po (pyrrhotite), py (pyrite), sp (sphalerite), tn-td (tennantite-tetrahedrite).

Samples from the feeder ore represent vein and replacement ore-types. The main ore minerals were galena and sphalerite (Figure 3E). Tetrahedrite, tennantite, and chalcopyrite were locally abundant (Figure 3F), whereas Pb-Ag-Cu sulfosalts were rare (Figure 3G). Carbonate reactive fronts were observed in the replacement ore (Figure 3H).

4.2. Fluid Inclusion Microthermometry

Sphalerite hosted two-phase primary FIs (H_2O -liquid and H_2O -vapor) at room temperatures. Their vapor proportion was approximately 10 vol.%. They clustered within a crystal or around cleavages. Their size in the feeder ore was $<1\text{--}50\ \mu\text{m}$, whereas that in the stratiform ore was up to $3\ \mu\text{m}$. Many FIs appeared to have necked down (Figure 4). In addition, FI paragenesis at the crystal scale was difficult to unravel, and thus the resolution of the FI assemblage was limited to the sample scale.

The T_m and T_h were obtained from the FIs hosted by sphalerite in samples 39-15 and 39-25 (Table 1). In the former, the T_m were $-3.7 \pm 0.4\ ^\circ\text{C}$ (1σ , $n = 26$) and the T_h were $165.3 \pm 5.4\ ^\circ\text{C}$ (1σ , $n = 31$). In the latter, the T_m were $-3.7 \pm 0.6\ ^\circ\text{C}$ (1σ , $n = 10$) and the T_h were $164.0 \pm 4.4\ ^\circ\text{C}$ (1σ , $n = 13$). The T_m in samples 39-15 and 39-25 corresponded to salinities of $6.0 \pm 0.6\ \text{wt.}\% \text{ NaCl equiv}$ (1σ) and $5.9 \pm 0.8\ \text{wt.}\% \text{ NaCl equiv}$ (1σ), respectively. The FIs from the stratiform ore were not analyzed due to their small size.

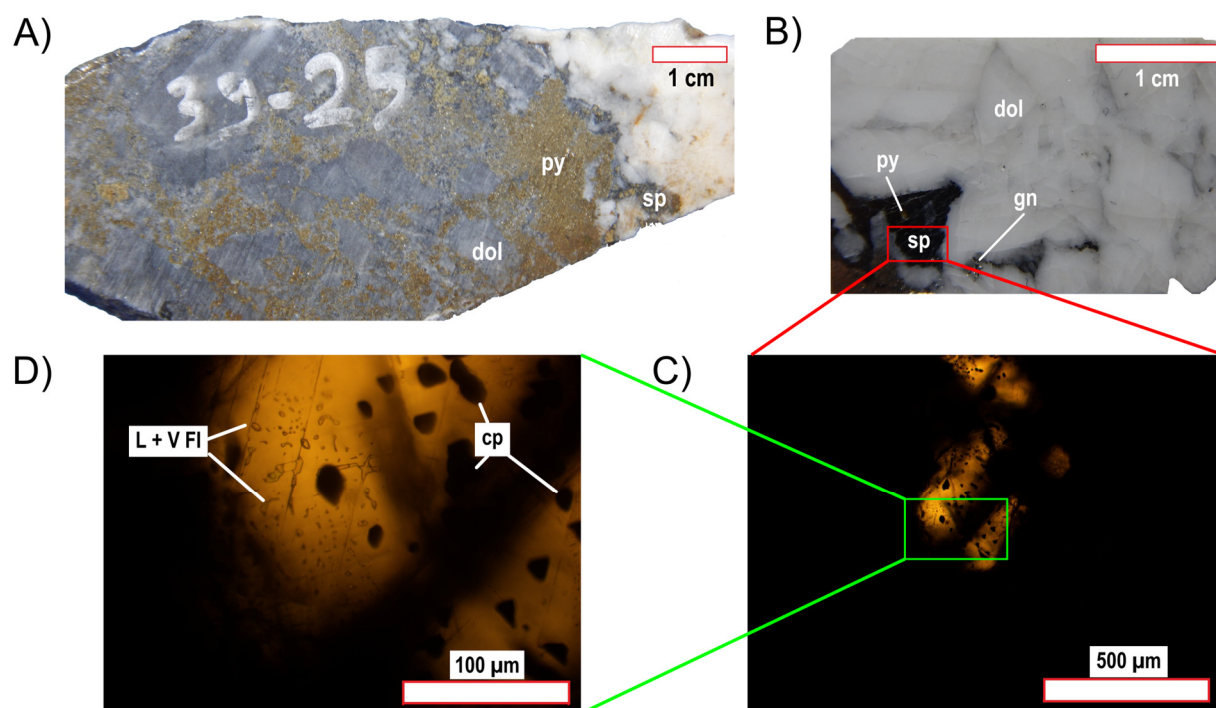


Figure 4. (A) Hand-specimen from which the fluid inclusion wafer in (B) was prepared. Sphalerite coexists with pyrite and is associated with galena and dolomite. (C) Sphalerite crystal where fluid inclusions in (D) are present. They occur in isolated clusters. Illumination is blocked by dark sphalerite and chalcopyrite blebs. Abbreviations: cp (chalcopyrite), dol (dolomite), gn (galena), sp (sphalerite), py (pyrite), L + V FI (liquid-vapor fluid inclusion).

Table 1. Results of fluid inclusion microthermometry.

Sample	Depth (m)	Host	FIA	No	T_m	Salinity	T_h
					(°C)	(wt.% NaCl equiv)	(°C)
39-25	146	Sphalerite	1	1	−3.3	5.4	168.2
				2	−4.4	7.1	158.1
				3	−4.6	7.3	165.5
				4			155.8
				5	−3.8	6.1	159.7
				6	−3.4	5.5	166.2
				7			166.5
				8	−3.3	5.4	158.1
				9	−3.3	5.4	167.3
				10	−3.2	5.3	168.3
				11			164.8
				12			166.7
				13			166.7
			<i>m</i>	−3.7	5.9	164.0	
			σ	0.6	0.8	4.4	
39-15	102	Sphalerite	1	1	−3.6	5.8	153.4
				2	−4.0	6.4	169.0
				3			166.8
				4	−3.9	6.2	163.7
				5	−3.6	5.8	161.3
				6	−4.2	6.8	166.5
				7	−3.8	6.1	172.2
				8	−3.6	5.8	167.4
				9	−4.1	6.7	167.3

Table 1. Cont.

Sample	Depth (m)	Host	FIA	No	T _m	Salinity	T _h
					(°C)	(wt.% NaCl equiv)	(°C)
				10			167.4
				11	−3.5	5.7	173.0
				12	−4.1	6.7	168.7
				13	−4.4	7.1	
				14	−3.8	6.1	172.0
				15	−3.5	5.7	
				16	−3.6	5.8	172.2
				17	−4.1	6.7	172.5
				18			164.5
				19			166.1
				20			162.0
				21			165.6
				22			161.6
				23			162.4
				24			163.4
				25			163.7
				26			164.5
				27	−3.8	6.1	156.9
				28	−3.5	5.7	151.7
				29	−3.5	5.7	
				30	−4.0	6.4	
				31	−3.3	5.4	168.0
				32	−4.1	6.5	
				33	−3.5	5.7	
				34	−4.4	7.1	
				35	−2.9	4.8	
				36	−3.1	5.1	
				37	−3.2	5.3	
				<i>m</i>	−3.7	6.0	165.3
				<i>σ</i>	0.4	0.6	5.4

4.3. Sphalerite Composition

Sphalerite from the feeder and stratiform ores had distinct Fe and Cu contents (Table 2). The former contained 0.7–3.2 wt.% Fe (1.2–5.6 mole% FeS; average = 3.4 mole% FeS) whereas the latter hosted 4.5–7.7 wt.% Fe (7.9–13.4 mole% FeS; average = 9.9 mole% FeS). Sphalerite in samples 6-09 and 58-24 (hosted by the feeder ore) contained 1.3 and 0.6 wt.% Cu, respectively. Aside from the Fe and Cu contents, sphalerite in all samples had low Cd (0.2–0.4 wt.%), Ga (<0.1 wt.%), and In (below detection limit) contents (Table 2).

Table 2. EPMA results on sphalerite chemical composition.

Sample	Ore	<i>n</i>	Zn	Fe	Cu	Cd	Ga	In	S	Total	Empirical Formulae
			wt.%								
104-11	Stratiform	8	61.19	5.87	b.d.l.	0.24	0.05	0.01	33.51	100.84	(Zn _{0.90} Fe _{0.10}) _{1.00} S _{1.00}
104-14	Stratiform	7	62.20	4.65	b.d.l.	0.26	0.05	b.d.l.	33.07	100.21	(Zn _{0.92} Fe _{0.08}) _{1.00} S _{1.00}
58-11	Stratiform	9	62.08	4.52	b.d.l.	0.29	0.04	b.d.l.	33.00	99.92	(Zn _{0.92} Fe _{0.08}) _{1.00} S _{1.00}
168-06	Stratiform	9	61.76	5.10	b.d.l.	0.22	0.05	b.d.l.	32.57	99.68	(Zn _{0.92} Fe _{0.09}) _{1.01} S _{0.99}
292-37	Stratiform	13	59.41	7.74	b.d.l.	0.23	0.04	0.01	32.71	100.11	(Zn _{0.88} Fe _{0.13}) _{1.01} S _{0.99}
44-11	Stratiform	7	60.56	6.42	b.d.l.	0.23	0.04	b.d.l.	33.30	100.53	(Zn _{0.89} Fe _{0.11}) _{1.00} S _{1.00}
58-24	Feeder	10	64.95	1.07	1.34	0.21	0.08	0.01	33.00	100.62	(Zn _{0.96} Fe _{0.02} Cu _{0.02}) _{1.00} S _{1.00}
39-06	Feeder	7	64.11	3.21	b.d.l.	0.31	0.05	b.d.l.	32.92	100.58	(Zn _{0.95} Fe _{0.06}) _{1.01} S _{0.99}
39-08	Feeder	7	66.44	0.90	b.d.l.	0.29	0.05	b.d.l.	32.92	100.59	(Zn _{0.99} Fe _{0.02}) _{1.01} S _{0.99}
39-15	Feeder	9	63.93	2.51	b.d.l.	0.29	0.06	b.d.l.	32.95	99.70	(Zn _{0.96} Fe _{0.04}) _{1.00} S _{1.00}
39-21	Feeder	4	64.88	2.31	b.d.l.	0.25	b.d.l.	0.01	32.94	100.38	(Zn _{0.96} Fe _{0.04}) _{1.00} S _{1.00}
39-24	Feeder	8	64.01	3.19	b.d.l.	0.35	0.05	b.d.l.	32.36	99.94	(Zn _{0.95} Fe _{0.06}) _{1.01} S _{0.99}
39-25	Feeder	5	65.95	1.61	b.d.l.	0.36	0.06	0.01	32.46	100.40	(Zn _{0.98} Fe _{0.03}) _{1.01} S _{0.99}
6-09	Feeder	9	66.13	0.69	0.62	0.16	0.04	0.01	32.90	100.52	(Zn _{0.98} Fe _{0.01} Cu _{0.01}) _{1.00} S _{1.00}

5. Discussion

5.1. Ore-Fluid Temperatures, Salinities, and Densities

Temperatures and salinities obtained from samples 39-15 and 39-25 were uniform, irrespective of their depth location (Table 1). The FIs in samples 39-15 and 39-25 homogenized at 165.3 ± 5.4 °C (1σ) and 164.0 ± 4.4 °C (1σ), respectively. Salinities were approximately 6.0 ± 0.6 wt.% NaCl equiv (1σ) in sample 39-15 and 5.9 ± 0.8 wt.% NaCl equiv (1σ) in sample 39-25. One explanation for these similarities is that the ore fluid ascended rapidly from its source, thus, minimizing heat loss to the wall rocks. However, given the unclear paragenesis between samples 39-15 and 39-25, sphalerite-bearing quartz veins in both samples could have formed from different batches of ore fluid that equilibrated with the source rocks at nearly equal temperatures.

Mixing between the ore fluid and marine sediment porewater gradually modified the ore-fluid densities from 0.96 g/mL to 1.02 g/mL as the proportion of the latter increased toward unity (Figure 5A). The initial and evolving densities of the Sopokomil ore fluid are lower than seawater density (Figure 5B), consistent with the idea that the ascent of an SHMS ore fluid is promoted by buoyancy when a channel connecting the source zone to the depositional site exists [31].

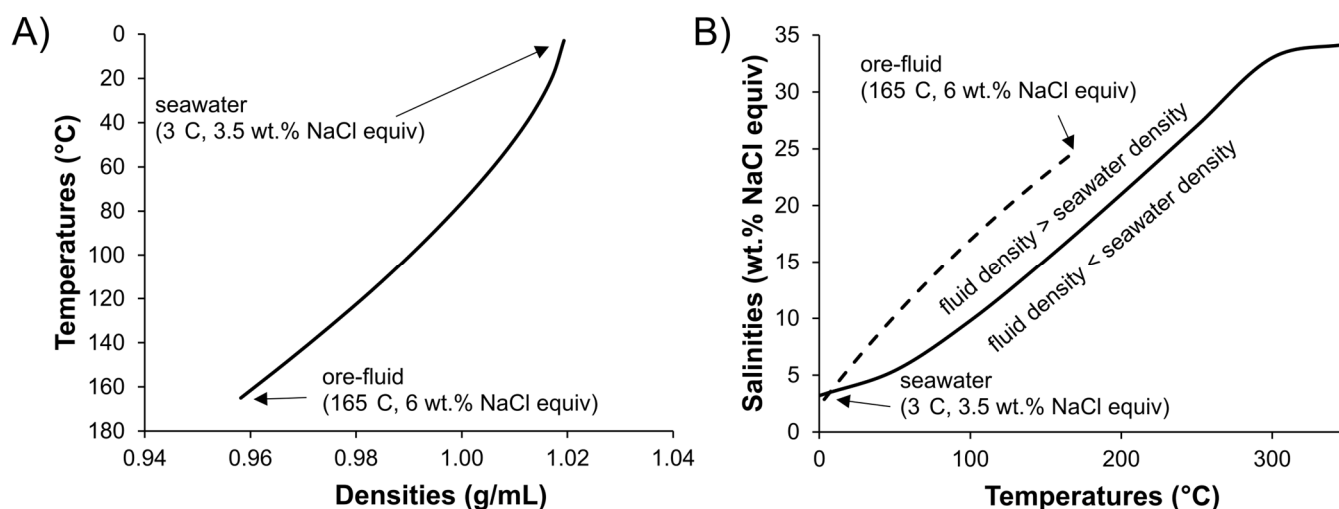


Figure 5. (A) Evolution of the Sopokomil ore-fluid densities due to dilution by seawater. (B) The Sopokomil ore-fluid densities vs. seawater densities at varying temperatures (calculated based on [32]).

5.2. Ore-Fluid Redox State and pH

It is generally accepted that redox state and pH of an SHMS ore fluid are determined by the rift-fill basin sequence [12,33], and probably the basement as well [34,35], in which its parent fluid circulates. At Sopokomil, even on Sumatra, direct observation of the rift-fill rocks cannot be made as they do not crop out [22]. Accordingly, the rift-fill sequence is inferred from the Pre-Carboniferous strata across the Indochina Terrane, to which the West Sumatra Block was attached during the Carboniferous. The strata are dominated by interbedded shale, sandstone, and siltstone; oxidized rocks including limestone and chert are minor [36]. This package, which resembles the mica-rich, carbonaceous matter-rich, sedimentary pyrite-bearing rocks hosting the Sopokomil Zn-Pb mineralization, may have rendered the crustal fluid reduced ($m\text{SO}_4^{2-} < m\text{H}_2\text{S}$) [12,37,38].

The reduced nature of the ore fluid at Sopokomil is further reflected in the chemistry of its sulfide products. First, the FeS contents in sphalerite from the feeder (3.4 mole% FeS) and stratiform (9.9 mole% FeS) ores suggest relatively low sulfur fugacity in the ore fluid ($\log f\text{S}_2 \approx -16.0$ to -18.1), corresponding to low oxygen fugacity ($\log f\text{O}_2 \approx -47.9$ to -50.0). Second, iron sulfides are present as pyrite and pyrrhotite. Third, there is no evidence that hematite or magnetite exists [7].

Due to its reduced condition, the Sopokomil ore fluid must have been acidic to be capable of transporting considerable Zn and Pb [12,14]. Table 3, which summarizes the ore-fluid pH calculation, suggests that the maximum pH should be 2.78 if the ore fluid contained 100 ppm Zn and 50 ppm Pb. In the ore fluid with 50 ppm Zn and 25 ppm Pb, the highest possible pH was 2.92. The likely maximum pH increased with decreasing Zn-Pb concentrations: (1) 3.12 at $\Sigma\text{Zn} = 20$ ppm and $\Sigma\text{Pb} = 10$ ppm, (2) 3.27 at $\Sigma\text{Zn} = 10$ ppm and $\Sigma\text{Pb} = 5$ ppm, and (3) 3.84 at $\Sigma\text{Zn} = 2$ ppm and $\Sigma\text{Pb} = 1$ ppm.

Table 3. Results of ore-fluid pH calculation.

Pb (ppm)	Zn (ppm)	pH	Galena ($\times 10^{-3}$ mg)	Sphalerite ($\times 10^{-3}$ mg)	Pb (ppm)	Zn (ppm)	pH	Galena ($\times 10^{-3}$ mg)	Sphalerite ($\times 10^{-3}$ mg)
50	100	2.86	16,384	0	5	10	3.48	2686	2517
		2.85	14,253	0			3.46	2511	201
		2.85	58	0			3.43	2234	17
		2.83	54	0			3.40	1908	0
		2.82	50	0			3.38	1557	0
		2.80	47	0			3.35	124	0
		2.79	44	0			3.33	49	0
		2.78	0	0			3.30	780	0
		2.76	0	0			3.27	0	0
		2.75	0	0			3.23	0	0
		2.74	0	0			3.19	0	0
		25	50	3.03			66	18	1
3.01	60			0	3.99	329	0		
2.98	54			0	3.94	203	0		
2.96	49			0	3.89	42	0		
2.94	45			0	3.84	0	0		
2.92	0			0	3.79	0	0		
2.91	0			0	3.74	0	0		
2.89	0			0	3.70	0	0		
2.87	0			0	3.65	0	0		
2.85	0			0	3.61	0	0		
2.84	0			0	3.58	0	0		
10	20			3.27	5315	4959			
		3.25	4834	2985					
		3.23	4563	47					
		3.20	3477	0					
		3.17	2212	0					
		3.15	46	0					
		3.12	0	0					
		3.09	0	0					
		3.06	0	0					
		3.04	0	0					
		3.01	0	0					

Compositional constraints: $\Sigma\text{Fe} = 10^{-3}$ m, $\Sigma\text{S} = 10^{-3}$ m, $\Sigma\text{C} = 0.256$ m, $T = 165$ °C, $P = 250$ bars, salinity = 6 wt.% NaCl equiv.

5.3. Metal Transport and Sulfide Deposition

It is argued that in acidic, S-deficient, moderately to highly saline hydrothermal fluids, Zn and Pb are mainly transported as chloride complexes [29,37,39–41]. In the Sopokomil ore fluid, ZnCl^+ and $\text{PbCl}_2(\text{aq})$ were the principal Zn- and Pb-chlorides, respectively (Figure 6A,B). Zn proportion occurring as ZnCl^+ was approximately 80%. Nearly 17% of Zn existed in $\text{ZnCl}_2(\text{aq})$, whereas the rest was present as Zn^{2+} and ZnCl_3^- . This order is in good agreement with other accounts [29,42]. Unlike the dominance of ZnCl^+ over the other Zn-chlorides, that of $\text{PbCl}_2(\text{aq})$ over the other Pb-chlorides was unclear. $\text{PbCl}_2(\text{aq})$ proportion was around 35%, only 7% and 9% above that of PbCl_3^- and PbCl_4^{2-} , respectively. The percentage of Pb transported as PbCl^+ was $\approx 11\%$, and as Pb^{2+} was $\approx 1\%$.

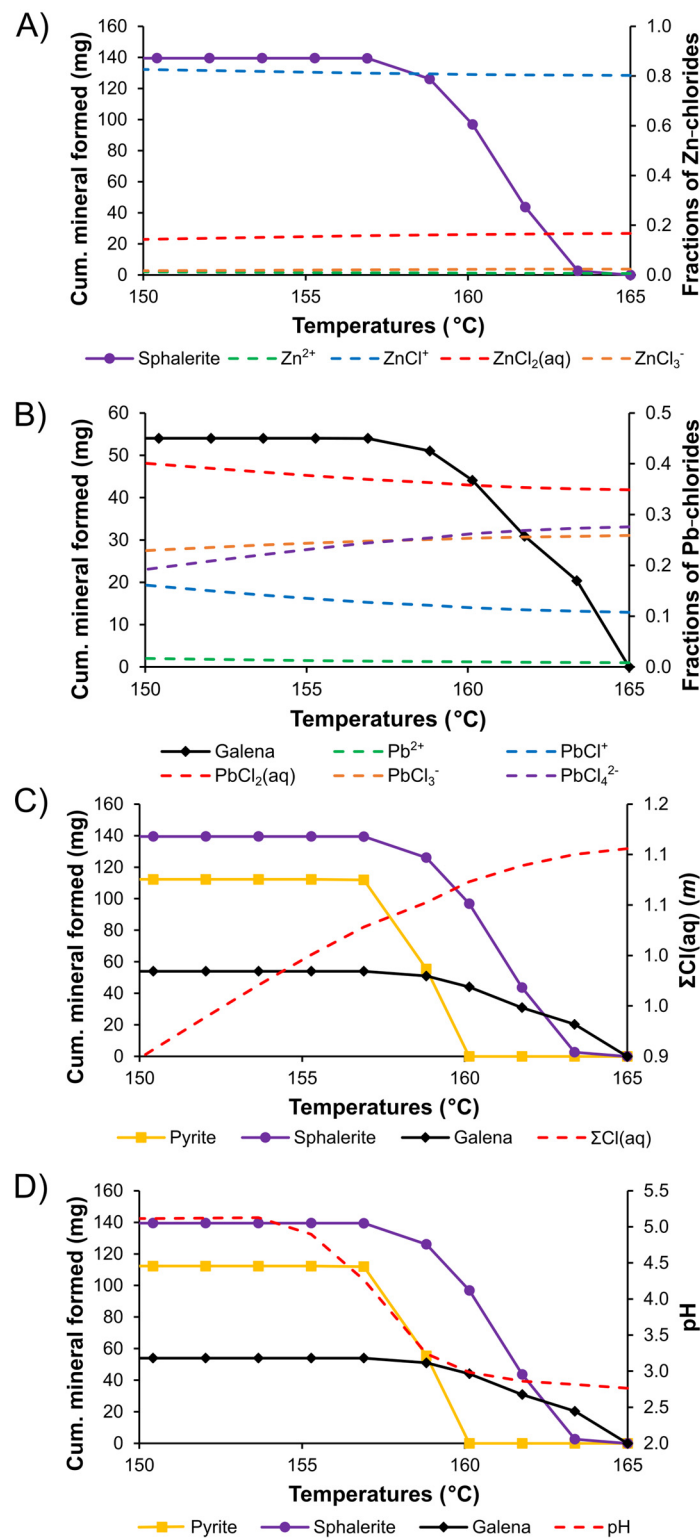


Figure 6. Speciation of (A) Zn-chlorides and (B) Pb-chlorides in the Sopokomil ore fluid. Evolution of (C) ΣCl and (D) pH with progressive dilution of 1 kg of ore fluid. Cumulative precipitating minerals are embedded in all graphs. Starting compositional constraints and results thermodynamic calculation are available in Tables A1 and A2.

Given the reduced and acidic conditions, sulfide precipitation at Sopokomil was most likely driven by mixing between the ore fluid and marine sediment porewater, a mechanism proposed for SHMS deposits, with reduced acidic ore fluids elsewhere [12–14].

Immediate consequences of mixing were that the Sopokomil ore fluid became less saline, less acidic, and cooler (Figure 6C,D, Table A2). The effects of ΣCl and pH changes on the sulfide precipitation can be explained by the reaction:



where Me represents Zn and Pb, n is an integer in $0 \leq n \leq 4$. The reaction shows that the decreased ΣCl and the increased pH at an isothermal condition favor the reactant side, destabilizing metal-chlorides in the evolving ore fluid. With decreasing temperatures, the equilibrium shifts to the left as its reaction constant becomes smaller (Table 4).

Table 4. Equilibrium constant of reactions involving sulfides and metal-chlorides.

Reaction	log K			
	150 °C	155 °C	160 °C	165 °C
$\text{sp}(\text{s}) + \text{Cl}^- + 2\text{H}^+ = \text{H}_2\text{S}(\text{aq}) + \text{ZnCl}^+$	−0.8077	−0.6736	−0.5399	−0.4063
$\text{gn}(\text{s}) + 2\text{Cl}^- + 2\text{H}^+ = \text{H}_2\text{S}(\text{aq}) + \text{PbCl}_2(\text{aq})$	−7.6769	−7.5247	−7.3757	−7.2298

Abbreviations: gn (galena), sp (sphalerite).

In terms of metal transport, progressive mixing made the primary Zn- and Pb-chlorides more pronounced despite the lower ΣCl in the aqueous phase (Figure 6A,B). Within a 15 °C change in the temperatures, the ZnCl^+ and $\text{PbCl}_2(\text{aq})$ proportions increased to 83% and 40%, respectively. The increases were balanced by decreases in their secondary counterparts: (1) $\text{ZnCl}_2(\text{aq})$ with respect to ZnCl^+ and (2) PbCl_3^- and PbCl_4^{2-} with respect to $\text{PbCl}_2(\text{aq})$.

The bulk of sulfides precipitated in the early stage of mixing (Figure 7A). $T = 165\text{--}160$ °C was the most critical temperatures for galena and sphalerite precipitation. Galena dominated at the onset of dilution, followed by major sphalerite precipitation toward the end of the temperature range. Within $T = 160\text{--}155$ °C, most sulfides precipitated as pyrite while sphalerite and galena continued to precipitate. At $T = 155\text{--}150$ °C, only trace amounts of sulfides were deposited despite the continuously increased ΣS (Figure 7B), probably due to the low ΣZn , ΣPb , and ΣFe in the residual ore fluid. The metal concentrations in the aqueous phase at $T = 155$ °C were five to six orders of magnitude lower than their original conditions, making the residual ore fluid undersaturated with respect to sphalerite, galena, and pyrite. The sulfide depositional sequence above is reflected in the two most prominent ore textures (Figure 7A). In the sphalerite-rich massive ore-type, sphalerite is dominant and intergrown by galena, whereas pyrite occurs in trace amounts. This accords with the modelled sulfide assemblage forming within $T = 165\text{--}160$ °C. In the pyrite-rich massive ore-type, pyrite and sphalerite are abundant, whereas galena is minor. This assemblage is in line with the modelling results at $T = 160\text{--}155$ °C.

The regimes of sulfide deposition are also mirrored by their Zn/Pb ratio (Figure 7A). The ratio was 0.1 at the onset of mixing, concurrent with the dominance of galena over sphalerite. It rose to 3.0 due to subsequent dilution, and steadily increased to 4.9 at $T = 154$ °C. Afterwards, the ratio jumped to 12.9, although only trace amounts of sulfides precipitated. The increased Zn/Pb ratio with progressive mixing is consistent with the report that galena is more abundant in the proximity of feeder zones [7].

It has been proposed that hydrothermal S carried by the ore fluid and bacteriogenic S dissolved in marine sediment porewater contribute to the precipitation of the Sopokomil sulfides [7]. The concept of dual S-sources is also implicated by our calculations. The initial ore fluid dissolved 0.001 *m* ΣS , which is hydrothermal in origin. In the beginning of the dilution, the proportion of hydrothermal S in the evolving ore fluid rapidly dropped to 53% when temperatures reached 162 °C. Progressive cooling to $T = 160$ °C and $T = 157$ °C further decreased the value to 32% and <10%, respectively (Figure 7C). If the ratio of hydrothermal and bacteriogenic S in the aqueous phase was the same to that in the solid phase, bacteriogenic S will account for 75% of S used in precipitating sulfides. This estimate

reinforces the results of previous S-isotope investigation, pointing out that S of bacteriogenic origin was responsible for the economic mineralization at Sopokomil [7].

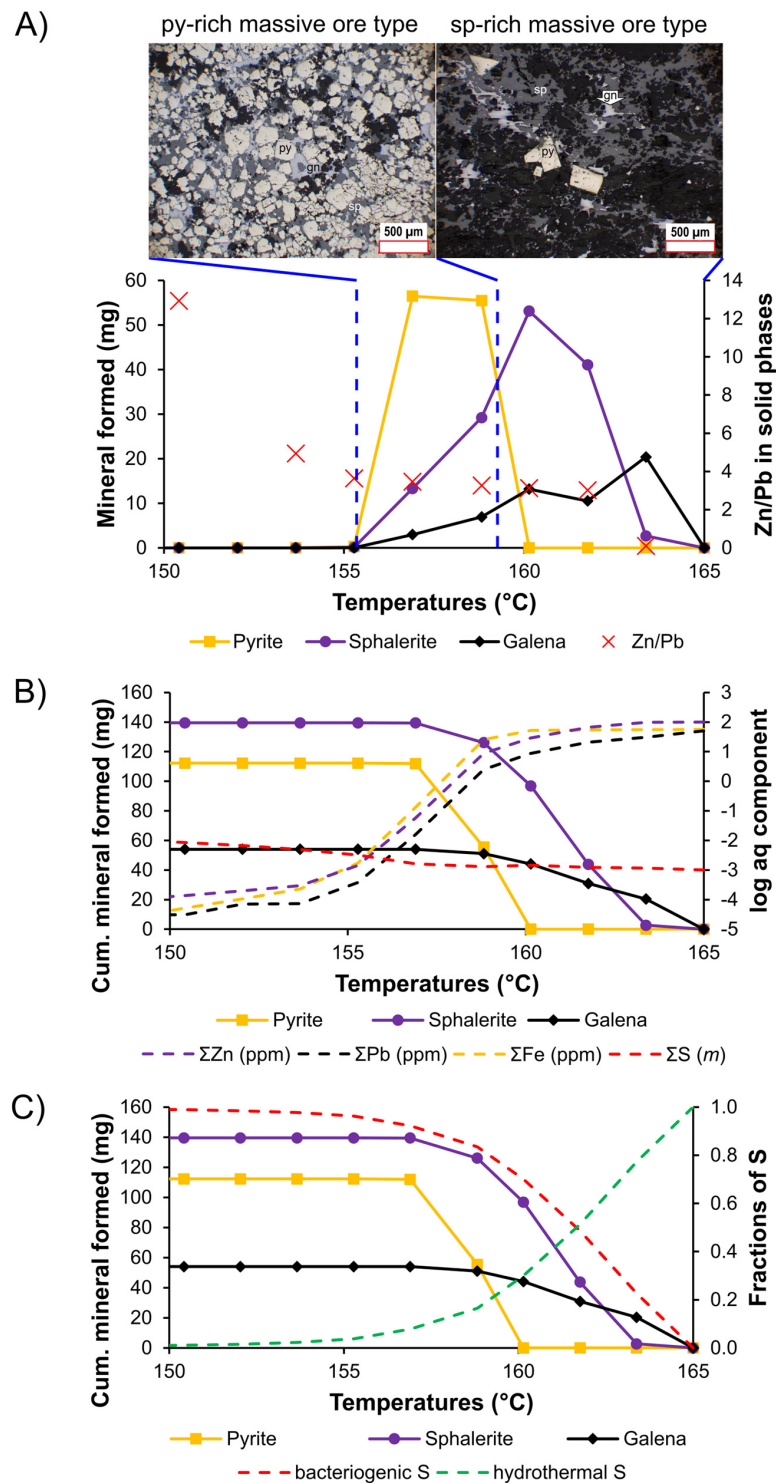


Figure 7. (A) Variation of Zn/Pb ratio and textures of ore products over the course of mixing compared to the amounts of sulfides precipitating from 1 kg of ore fluid. (B) Σ Zn, Σ Pb, Σ Fe, and Σ S in the evolving ore fluid. (C) Contribution of bacteriogenic and hydrothermal S to sulfides at Sopokomil. Cumulative precipitating minerals from 1 kg of ore fluid are embedded in (B,C). Starting compositional constraints and thermodynamic calculation are available in Tables A1 and A2. Abbreviations: gn (galena), sp (sphalerite), py (pyrite).

5.4. Genetic Model

The genesis of the Sopokomil SHMS Zn-Pb deposit is divided into two stages: ore-fluid preparation and mineralization (Figure 8). In the first stage, a precursor fluid circulated within a reduced rock package in the rift-fill basin sequence, equilibrating to reduced, acidic conditions with moderate temperatures and salinities (Figure 8A,B). The fluid with a sufficient Zn- and Pb-bearing capacity interacted with the reservoir rocks and leached their metals, resulting in a fertile ore fluid (Figure 8B,C). Having ascended to subseafloor environment, the ore fluid encountered cold marine sediment porewater with contrasting chemistry, marking the onset of the mineralization stage (Figure 8D,E). Their interaction disturbed thermal and chemical equilibrium in the ore fluid, prompting sulfide precipitation. At the start, galena and sphalerite were the dominant sulfide phases. With progressive dilution, pyrite became dominant and co-precipitated with sphalerite and minor galena. Sulfide deposition consumed S, mainly bacteriogenic in origin. The bulk of sulfides at Sopokomil formed within a narrow temperature range, when only a fraction of diluting agent involved (Figure 8E). The mineralization stage terminated as the residual fluid became undersaturated with respect to the sulfides (Figure 8F). The genetic concept above underscores the significance of steep thermal and chemical gradients generated by the ore-fluid dilution to the growth of the Sopokomil SHMS Zn-Pb deposit.

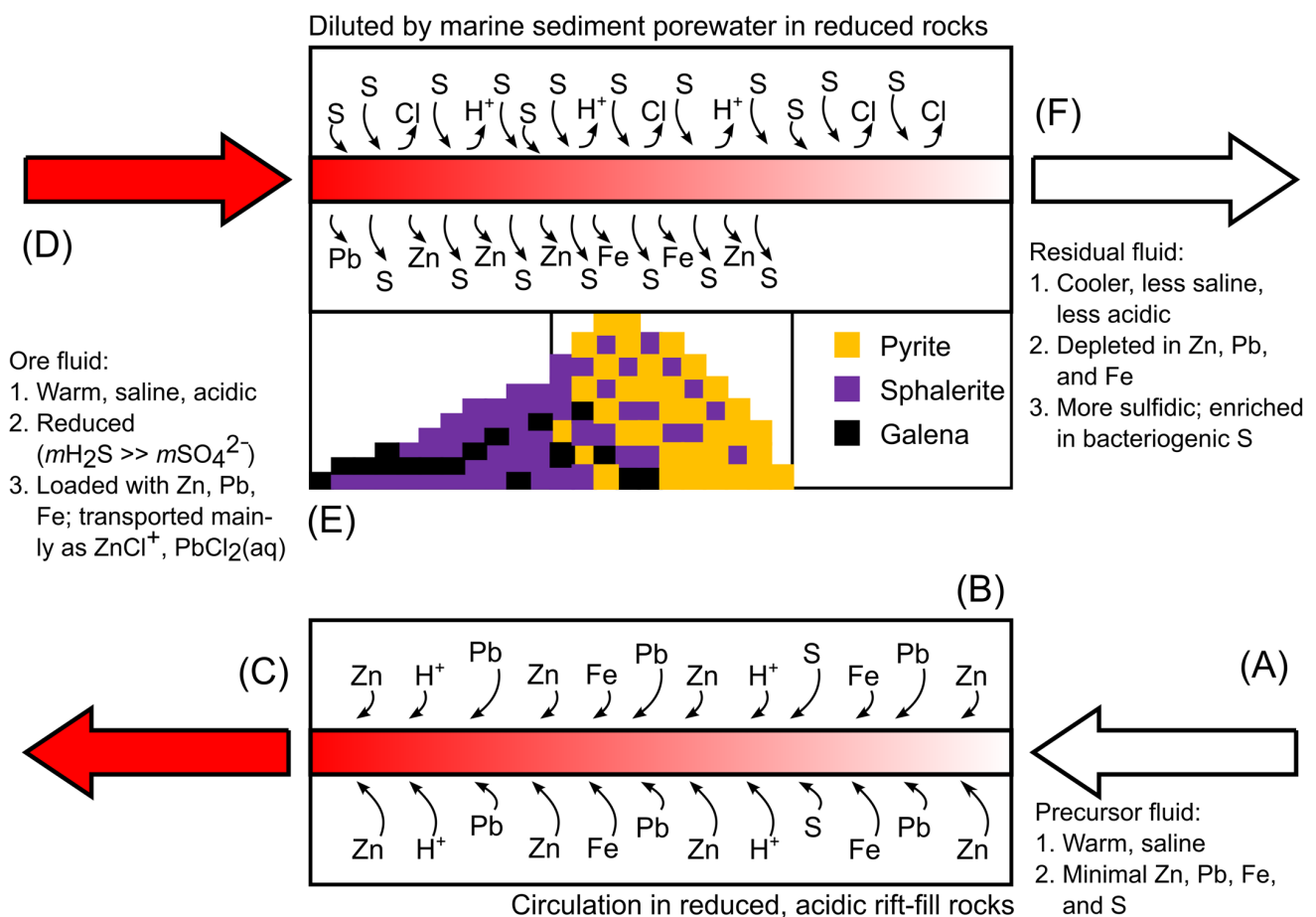


Figure 8. Conceptual genetic model of the Sopokomil SHMS Zn-Pb deposit. (A) A precursor fluid entered a source zone within the rift-fill sequence. (B) It circulated in the reservoir, extracting metals, and producing (C) a reduced, acidic ore fluid. (D) On arriving at the depositional site, (E) the ore fluid was diluted by marine sediment porewater resulting in sulfide precipitates. (F) The continuous dilution rendered the residual fluid undersaturated with respect to the sulfides, cooler, less saline, near neutral, and more sulfidic.

6. Conclusions

The ore-forming fluid in the Sopokomil Zn-Pb SHMS deposit was moderate in salinities (≈ 6 wt.% NaCl equiv) and temperatures (≈ 165 °C). These parameters correspond to a fluid less dense than seawater (≈ 0.96 g/mL). Zn and Pb were transported mainly as ZnCl^+ and $\text{PbCl}_2(\text{aq})$, respectively. Having been diluted by marine sediment porewater, the reduced acidic ore fluid at Sopokomil precipitated sulfides, mostly within $T = 165\text{--}155$ °C. The order of dominant sulfides precipitating from the evolving ore fluid produced a Zn/Pb ratio that increased with progressive mixing. Furthermore, the mixing model confirms that S supplied by marine sediment porewater was a crucial component in the sulfide deposition at Sopokomil. This study highlights the importance of a dramatic shift in thermal and chemical equilibrium in the early stage of mixing to the formation of the first significant SHMS deposit on Sumatra, and in Indonesia.

Author Contributions: Conceptualization, T.A.R., S., K.Y., and K.W.; methodology, T.A.R., K.Y., and K.S.; investigation, T.A.R., S., and K.Y.; formal analysis, T.A.R. and K.S.; modelling, T.A.R.; validation and interpretation, T.A.R., S., K.Y., K.S., and K.W.; resources, T.A.R., S., K.Y., K.S., and K.W.; data curation, T.A.R.; writing—original draft preparation, T.A.R.; writing—review and editing, S., K.Y., K.S., and K.W.; visualization, T.A.R.; supervision, K.Y. and K.W.; project administration, T.A.R.; funding acquisition, T.A.R., K.Y., and K.W. All authors have read and agreed to the published version of the manuscript.

Funding: This work was partially supported by funding from Advanced Graduate Program in Global Strategy for Green Asia (Kyushu University, Japan), the Society of Resource Geology (Japan), JSPS KAKENHI Grand-in-Aid for Scientific Research(B) Grant Number JP18H01927 (Japan), and JSPS Core-to-Core Program Grant Number JPJSCCB20200004.

Institutional Review Board Statement: Not applicable.

Informed Consent Statement: Not applicable.

Data Availability Statement: Data regarding FI microthermometry and sphalerite composition are available in the text body. Detail results of thermodynamic modelling are available in the Appendix A.

Acknowledgments: We are immensely grateful to PT Dairi Prima Mineral for the permission to collect samples and research the deposit. Thomas Tindell, Akira Imai, and (emeritus) Takushi Yokoyama are thanked for their constructive comments.

Conflicts of Interest: The authors declare no conflict of interests.

Appendix A

Table A1. Bulk composition of initial ore fluid and marine sediment porewater.

		Initial Ore Fluid	Marine Sediment Porewater
ΣC	(<i>m</i>)	0.256	0.002331235
ΣCa	(<i>m</i>)	0.031205	0.010255003
ΣCl	(<i>m</i>)	1.10103	0.54720335
ΣFe	(<i>m</i>)	0.001	6.09×10^{-8}
ΣH	(<i>m</i>)	111.02555	109.1324
ΣK	(<i>m</i>)	0.093614	0.010026011
ΣMg	(<i>m</i>)	3.12×10^{-5}	0.053075498
ΣNa	(<i>m</i>)	0.936142	0.46977356
ΣO	(<i>m</i>)	55.508373	55.189569
ΣPb	(<i>m</i>)	0.000241313	1.45×10^{10}
ΣS	(<i>m</i>)	0.001	0.028190974
ΣZn	(<i>m</i>)	0.00153	7.65×10^{-8}

Table A2. Results of thermodynamic calculation.

Run		1	2	3	4	5	6	7	8	9	10	11
<i>Input</i>												
Porewater / ore fluid	(kg/kg)	0.00	0.01	0.02	0.03	0.04	0.05	0.06	0.07	0.08	0.09	0.10
Ore fluid	(kg)	1.00	1.00	1.01	1.03	1.06	1.10	1.16	1.23	1.31	1.42	1.55
Porewater	(kg)	0.00	0.01	0.02	0.03	0.04	0.06	0.07	0.09	0.11	0.13	0.15
T	(°C)	165	163	162	160	159	157	155	154	152	150	149
P	(bar)	250	250	250	250	250	250	250	250	250	250	250
<i>Output</i>												
Aqueous phase	(kg)	1.00	1.01	1.03	1.06	1.10	1.16	1.23	1.31	1.42	1.55	1.70
Ca ²⁺	(m)	2.2 × 10 ⁻²	2.2 × 10 ⁻²	2.1 × 10 ⁻²	2.1 × 10 ⁻²	2.1 × 10 ⁻²	2.0 × 10 ⁻²	2.0 × 10 ⁻²	1.9 × 10 ⁻²	1.8 × 10 ⁻²	1.6 × 10 ⁻²	1.5 × 10 ⁻²
CaCl ⁺	(m)	9.2 × 10 ⁻³	8.9 × 10 ⁻³	8.6 × 10 ⁻³	8.3 × 10 ⁻³	7.9 × 10 ⁻³	7.4 × 10 ⁻³	6.9 × 10 ⁻³	6.4 × 10 ⁻³	5.7 × 10 ⁻³	5.0 × 10 ⁻³	4.4 × 10 ⁻³
CaCl ₂	(m)	6.6 × 10 ⁻⁴	6.4 × 10 ⁻⁴	6.1 × 10 ⁻⁴	5.8 × 10 ⁻⁴	5.4 × 10 ⁻⁴	5.0 × 10 ⁻⁴	4.6 × 10 ⁻⁴	4.1 × 10 ⁻⁴	3.6 × 10 ⁻⁴	3.1 × 10 ⁻⁴	2.6 × 10 ⁻⁴
Fe ²⁺	(m)	7.5 × 10 ⁻⁴	7.5 × 10 ⁻⁴	7.4 × 10 ⁻⁴	7.2 × 10 ⁻⁴	3.5 × 10 ⁻⁴	1.8 × 10 ⁻⁴	2.4 × 10 ⁻⁸	3.2 × 10 ⁻⁹	1.5 × 10 ⁻⁹	7.4 × 10 ⁻¹⁰	3.5 × 10 ⁻¹⁰
FeCl ⁺	(m)	2.5 × 10 ⁻⁴	2.5 × 10 ⁻⁴	2.4 × 10 ⁻⁴	2.3 × 10 ⁻⁴	1.1 × 10 ⁻⁴	5.4 × 10 ⁻⁷	6.8 × 10 ⁻⁹	8.9 × 10 ⁻¹⁰	3.9 × 10 ⁻¹⁰	1.9 × 10 ⁻¹⁰	8.5 × 10 ⁻¹¹
FeCl ₂	(m)	4.0 × 10 ⁻⁷	3.5 × 10 ⁻⁷	3.0 × 10 ⁻⁷	2.5 × 10 ⁻⁷	1.0 × 10 ⁻⁷	4.6 × 10 ⁻¹⁰	5.0 × 10 ⁻¹²	5.7 × 10 ⁻¹³	2.2 × 10 ⁻¹³	9.1 × 10 ⁻¹⁴	3.6 × 10 ⁻¹⁴
K ⁺	(m)	9.2 × 10 ⁻²	9.2 × 10 ⁻²	9.0 × 10 ⁻²	8.8 × 10 ⁻²	8.5 × 10 ⁻²	8.1 × 10 ⁻²	7.7 × 10 ⁻²	7.2 × 10 ⁻²	6.8 × 10 ⁻²	6.3 × 10 ⁻²	5.8 × 10 ⁻²
KCl	(m)	1.7 × 10 ⁻³	1.6 × 10 ⁻³	1.6 × 10 ⁻³	1.5 × 10 ⁻³	1.3 × 10 ⁻³	1.2 × 10 ⁻³	1.1 × 10 ⁻³	1.0 × 10 ⁻³	8.9 × 10 ⁻⁴	7.8 × 10 ⁻⁴	6.8 × 10 ⁻⁴
Mg ²⁺	(m)	2.4 × 10 ⁻⁵	4.5 × 10 ⁻⁴	1.3 × 10 ⁻³	2.5 × 10 ⁻³	4.1 × 10 ⁻³	6.1 × 10 ⁻³	8.3 × 10 ⁻³	1.1 × 10 ⁻²	1.2 × 10 ⁻²	1.4 × 10 ⁻²	1.6 × 10 ⁻²
MgCl ⁺	(m)	7.0 × 10 ⁻⁶	1.3 × 10 ⁻⁴	3.6 × 10 ⁻⁴	6.8 × 10 ⁻⁴	1.1 × 10 ⁻³	1.5 × 10 ⁻³	2.0 × 10 ⁻³	2.5 × 10 ⁻³	2.8 × 10 ⁻³	3.1 × 10 ⁻³	3.4 × 10 ⁻³
Na ⁺	(m)	7.9 × 10 ⁻¹	7.9 × 10 ⁻¹	7.9 × 10 ⁻¹	7.8 × 10 ⁻¹	7.7 × 10 ⁻¹	7.5 × 10 ⁻¹	7.4 × 10 ⁻¹	7.2 × 10 ⁻¹	7.0 × 10 ⁻¹	6.8 × 10 ⁻¹	6.6 × 10 ⁻¹
NaCl	(m)	1.5 × 10 ⁻¹	1.4 × 10 ⁻¹	1.4 × 10 ⁻¹	1.3 × 10 ⁻¹	1.3 × 10 ⁻¹	1.2 × 10 ⁻¹	1.2 × 10 ⁻¹	1.1 × 10 ⁻¹	1.0 × 10 ⁻¹	9.5 × 10 ⁻²	8.9 × 10 ⁻²
pl ₂ ⁺	(m)	2.1 × 10 ⁻⁶	1.3 × 10 ⁻⁶	9.5 × 10 ⁻⁷	4.2 × 10 ⁻⁷	1.3 × 10 ⁻⁷	8.8 × 10 ⁻¹⁰	2.3 × 10 ⁻¹¹	4.9 × 10 ⁻¹²	5.2 × 10 ⁻¹²	2.5 × 10 ⁻¹²	2.7 × 10 ⁻¹²
PbCl ⁺	(m)	2.6 × 10 ⁻⁵	1.6 × 10 ⁻⁵	1.1 × 10 ⁻⁵	4.9 × 10 ⁻⁶	1.5 × 10 ⁻⁶	9.6 × 10 ⁻⁹	2.4 × 10 ⁻¹⁰	5.0 × 10 ⁻¹¹	5.1 × 10 ⁻¹¹	2.4 × 10 ⁻¹¹	2.5 × 10 ⁻¹¹
PbCl ₂	(m)	8.5 × 10 ⁻⁵	5.2 × 10 ⁻⁵	3.6 × 10 ⁻⁵	1.5 × 10 ⁻⁵	4.4 × 10 ⁻⁶	2.8 × 10 ⁻⁸	6.8 × 10 ⁻¹⁰	1.4 × 10 ⁻¹⁰	1.3 × 10 ⁻¹⁰	5.9 × 10 ⁻¹¹	6.0 × 10 ⁻¹¹
PbCl ₃ ⁻	(m)	6.3 × 10 ⁻⁵	3.8 × 10 ⁻⁵	2.6 × 10 ⁻⁵	1.1 × 10 ⁻⁵	3.1 × 10 ⁻⁶	1.9 × 10 ⁻⁸	4.4 × 10 ⁻¹⁰	8.6 × 10 ⁻¹¹	8.0 × 10 ⁻¹¹	3.4 × 10 ⁻¹¹	3.3 × 10 ⁻¹¹
PbCl ₄ ²⁻	(m)	6.7 × 10 ⁻⁵	4.1 × 10 ⁻⁵	2.7 × 10 ⁻⁵	1.1 × 10 ⁻⁵	3.1 × 10 ⁻⁶	1.9 × 10 ⁻⁸	4.2 × 10 ⁻¹⁰	7.9 × 10 ⁻¹¹	7.1 × 10 ⁻¹¹	2.9 × 10 ⁻¹¹	2.7 × 10 ⁻¹¹
Zn ²⁺	(m)	9.6 × 10 ⁻⁶	9.9 × 10 ⁻⁶	7.3 × 10 ⁻⁶	3.4 × 10 ⁻⁶	1.1 × 10 ⁻⁶	7.7 × 10 ⁻⁹	2.1 × 10 ⁻¹⁰	4.8 × 10 ⁻¹¹	3.5 × 10 ⁻¹¹	2.6 × 10 ⁻¹¹	2.1 × 10 ⁻¹¹
ZnCl ⁺	(m)	1.2 × 10 ⁻³	1.2 × 10 ⁻³	8.2 × 10 ⁻⁴	3.6 × 10 ⁻⁴	1.1 × 10 ⁻⁴	7.1 × 10 ⁻⁷	1.8 × 10 ⁻⁸	3.7 × 10 ⁻⁹	2.5 × 10 ⁻⁹	1.7 × 10 ⁻⁹	1.3 × 10 ⁻⁹
ZnCl ₂	(m)	2.6 × 10 ⁻⁴	2.5 × 10 ⁻⁴	1.7 × 10 ⁻⁴	7.2 × 10 ⁻⁵	2.1 × 10 ⁻⁵	1.4 × 10 ⁻⁷	3.4 × 10 ⁻⁹	6.9 × 10 ⁻¹⁰	4.5 × 10 ⁻¹⁰	3.1 × 10 ⁻¹⁰	2.2 × 10 ⁻¹⁰
ZnCl ₃ ⁻	(m)	3.6 × 10 ⁻⁵	3.5 × 10 ⁻⁵	2.4 × 10 ⁻⁵	1.0 × 10 ⁻⁵	3.0 × 10 ⁻⁶	1.9 × 10 ⁻⁸	4.5 × 10 ⁻¹⁰	8.9 × 10 ⁻¹¹	5.6 × 10 ⁻¹¹	3.7 × 10 ⁻¹¹	2.5 × 10 ⁻¹¹
CO ₂	(m)	1.3 × 10 ⁻¹										
CO ₃ ²⁻	(m)	8.5 × 10 ⁻¹²	1.1 × 10 ⁻¹¹	1.4 × 10 ⁻¹¹	2.6 × 10 ⁻¹¹	9.0 × 10 ⁻¹¹	1.0 × 10 ⁻⁸	1.9 × 10 ⁻⁷	5.6 × 10 ⁻⁷	5.5 × 10 ⁻⁷	5.5 × 10 ⁻⁷	5.6 × 10 ⁻⁷
HCO ₃ ⁻	(m)	2.5 × 10 ⁻⁵	3.0 × 10 ⁻⁵	3.4 × 10 ⁻⁵	4.7 × 10 ⁻⁵	8.7 × 10 ⁻⁵	9.4 × 10 ⁻⁴	4.1 × 10 ⁻³	7.1 × 10 ⁻³	7.2 × 10 ⁻³	7.3 × 10 ⁻³	7.4 × 10 ⁻³
CH ₄	(m)	1.3 × 10 ⁻¹	1.3 × 10 ⁻¹	1.2 × 10 ⁻¹	1.1 × 10 ⁻¹	1.0 × 10 ⁻¹	8.9 × 10 ⁻²	7.5 × 10 ⁻²	5.9 × 10 ⁻²	4.3 × 10 ⁻²	2.6 × 10 ⁻²	9.3 × 10 ⁻³
Cl ⁻	(m)	9.4 × 10 ⁻¹	9.4 × 10 ⁻¹	9.4 × 10 ⁻¹	9.1 × 10 ⁻¹	9.1 × 10 ⁻¹	8.9 × 10 ⁻¹	8.7 × 10 ⁻¹	8.5 × 10 ⁻¹	8.3 × 10 ⁻¹	8.0 × 10 ⁻¹	7.8 × 10 ⁻¹
HCl	(m)	3.3 × 10 ⁻⁴	2.8 × 10 ⁻⁴	2.5 × 10 ⁻⁴	1.8 × 10 ⁻⁴	9.7 × 10 ⁻⁵	8.9 × 10 ⁻⁶	2.0 × 10 ⁻⁶	1.1 × 10 ⁻⁶	1.1 × 10 ⁻⁶	1.1 × 10 ⁻⁶	1.0 × 10 ⁻⁶
H ₂	(m)	9.0 × 10 ⁻⁶	8.3 × 10 ⁻⁶	7.6 × 10 ⁻⁶	6.9 × 10 ⁻⁶	6.3 × 10 ⁻⁶	5.6 × 10 ⁻⁶	5.0 × 10 ⁻⁶	4.4 × 10 ⁻⁶	3.8 × 10 ⁻⁶	3.1 × 10 ⁻⁶	2.3 × 10 ⁻⁶
O ₂	(m)	0.00	0.00	0.00	0.00	0.00	0.00	0.00	0.00	0.00	0.00	0.00
HSO ₄ ⁻	(m)	5.3 × 10 ⁻¹⁶	7.1 × 10 ⁻¹⁶	8.6 × 10 ⁻¹⁶	1.4 × 10 ⁻¹⁵	2.6 × 10 ⁻¹⁵	3.7 × 10 ⁻¹⁴	3.5 × 10 ⁻¹³	1.1 × 10 ⁻¹²	2.0 × 10 ⁻¹²	4.0 × 10 ⁻¹²	1.3 × 10 ⁻¹¹
SO ₄ ²⁻	(m)	3.4 × 10 ⁻¹⁶	5.3 × 10 ⁻¹⁶	7.5 × 10 ⁻¹⁶	1.7 × 10 ⁻¹⁵	5.8 × 10 ⁻¹⁵	9.2 × 10 ⁻¹³	3.9 × 10 ⁻¹¹	2.1 × 10 ⁻¹⁰	3.9 × 10 ⁻¹⁰	8.1 × 10 ⁻¹⁰	2.8 × 10 ⁻⁹
H ₂ S	(m)	1.0 × 10 ⁻³	1.2 × 10 ⁻³	1.2 × 10 ⁻³	1.4 × 10 ⁻³	1.3 × 10 ⁻³	1.6 × 10 ⁻³	3.0 × 10 ⁻³	4.5 × 10 ⁻³	6.1 × 10 ⁻³	7.8 × 10 ⁻³	9.5 × 10 ⁻³
HS ⁻	(m)	3.9 × 10 ⁻⁷	5.2 × 10 ⁻⁷	6.2 × 10 ⁻⁷	9.7 × 10 ⁻⁷	1.6 × 10 ⁻⁶	2.1 × 10 ⁻⁵	1.7 × 10 ⁻⁴	4.2 × 10 ⁻⁴	5.7 × 10 ⁻⁴	7.2 × 10 ⁻⁴	8.7 × 10 ⁻⁴
OH ⁻	(m)	3.7 × 10 ⁻⁹	4.1 × 10 ⁻⁹	4.4 × 10 ⁻⁹	5.6 × 10 ⁻⁹	9.8 × 10 ⁻⁹	9.9 × 10 ⁻⁸	4.1 × 10 ⁻⁷	6.7 × 10 ⁻⁷	6.4 × 10 ⁻⁷	6.1 × 10 ⁻⁷	5.8 × 10 ⁻⁷
H ⁺	(m)	3.0 × 10 ⁻³	2.6 × 10 ⁻³	2.4 × 10 ⁻³	1.8 × 10 ⁻³	9.7 × 10 ⁻⁴	9.2 × 10 ⁻⁵	2.1 × 10 ⁻⁵	1.3 × 10 ⁻⁵			
H ₂ O	(m)	5.6 × 10 ¹										
<i>Gas phase</i>												
log fCO ₂	(kg)	0.00	0.00	0.00	0.00	0.00	0.00	0.00	0.00	0.00	0.00	0.00
log fCH ₄		1.32	1.32	1.33	1.33	1.33	1.33	1.32	1.32	1.32	1.32	1.32
log fH ₂		2.21	2.21	2.20	2.17	2.13	2.08	2.01	1.91	1.78	1.57	1.12
log fH ₂ S		-1.97	-2.00	-2.03	-2.06	-2.10	-2.14	-2.19	-2.24	-2.30	-2.38	-2.52
log fO ₂		-47.29	-47.49	-47.67	-47.85	-48.03	-48.21	-48.37	-48.53	-48.67	-48.77	-48.75
log fS ₂		-14.61	-14.50	-14.47	-14.34	-14.43	-14.25	-13.69	-13.34	-13.03	-12.74	-12.37
<i>Solid phase</i>												
Calcite	(mg)	0.000	0.000	0.000	0.000	0.000	0.000	0.000	0.000	0.000	0.000	0.000
Dolomite	(mg)	0.000	0.000	0.000	0.000	0.000	0.000	0.000	28.072	232.478	279.723	335.312
Pyrite	(mg)	0.000	0.000	0.000	0.000	55.489	56.462	0.303	0.004	0.001	0.001	0.001
Pyrrhotite	(mg)	0.000	0.000	0.000	0.000	0.000	0.000	0.000	0.000	0.000	0.000	0.000
Galena	(mg)	0.000	20.379	10.526	13.178	6.936	2.983	0.019	0.000	0.000	0.000	0.000
Sphalerite	(mg)	0.000	2.674	41.071	53.120	29.221	13.321	0.090	0.003	0.001	0.001	0.001

References

- ESDM One Map. Available online: <https://geoportal.esdm.go.id/> (accessed on 28 April 2021).
- Emsbo, P.; Seal, R.R.; Breit, G.N.; Diehl, S.F.; Shah, A.K. *Sedimentary Exhalative (Sedex) Zinc-Lead-Silver Deposit Model: U.S. Geological Survey Scientific Investigations Report 2010-5070-N*; U.S. Geological Survey: Reston, VA, USA, 2016. [CrossRef]
- Crow, M.J.; van Leeuwen, T.M. Metallic mineral deposits. In *Sumatra: Geology, Resources and Tectonic Evolution*; Barber, A.J., Crow, M.J., Milsom, J., Eds.; The Geological Society: Bath, UK, 2005; pp. 147–174. [CrossRef]
- van Leeuwen, T. A Brief History of Mineral Exploration and Mining in Sumatra. In Proceedings of the Proceedings of Sundaland Resources 2014 MGEI Annual Convention, Palembang, Indonesia, 17–18 November 2014; pp. 35–57.
- Harahap, B.H.; Abidin, H.Z.; Gunawan, W.; Yuniarni, R. Genesis of Pb-Zn-Cu-Ag Deposits within Permian Carboniferous-Carbonate Rocks in Madina Regency, North Sumatra. *Indones. J. Geosci.* **2015**, *2*, 167–184. [CrossRef]
- Abidin, H.Z.; Utoyo, H. Mineralization of the Selected Base Metal Deposits in the Barisan Range, Sumatera, Indonesia (Case Study at Lokop, Dairi, Latong, Tanjung Balit and Tuboh). *Indones. Min. J.* **2014**, *17*, 122–133.
- Rivai, T.A.; Syafrizal; Yonezu, K.; Tindell, T.; Boyce, A.J.; Sanematsu, K.; Satori, S.; Watanabe, K. The Dairi SEDEX Zn + Pb + Ag Deposit (North Sumatra, Indonesia): Insights from Mineralogy and Sulfur Isotope Systematics. *Ore. Geol. Rev.* **2020**, *122*, 103510. [CrossRef]
- Rivai, T.A.; Yonezu, K.; Tindell, T.; Imai, A.; Watanabe, K.; Syafrizal; Boyce, A.J. Dairi: An Example of Zn-Pb-Ag Sediment-Hosted Deposit from Indonesia. In Proceedings of the 15th SGA Biennial Meeting on Life with Ore Deposits on Earth, Glasgow, Scotland, 27–30 August 2019; pp. 25–32.
- Huston, D.L.; Large, R.R. Genetic and Exploration Significance of the Zinc Ratio (100 Zn/(Zn + Pb)) in Massive Sulfide Systems. *Econ. Geol.* **1987**, *82*, 1521–1539. [CrossRef]

10. Leach, D.L.; Sangster, D.F.; Kelley, K.D.; Large, R.R.; Garven, G.; Allen, C.R.; Gutzmer, J.; Walters, S. Sediment-hosted lead-zinc deposits: A global perspective. In *Economic Geology 100th Anniversary Volume*; Hedenquist, J.W., Thompson, J.F.H., Goldfarb, R.J., Richards, J.P., Eds.; Society of Economic Geologists, Inc.: Littleton, CO, USA, 2005; pp. 561–607.
11. Leach, D.L.; Marsh, E.; Emsbo, P.; Rombach, C.S.; Kelley, K.D.; Anthony, M. Nature of Hydrothermal Fluids at the Shale-Hosted Red Dog Zn-Pb-Ag Deposits, Brooks Range, Alaska. *Econ. Geol.* **2004**, *99*, 1449–1480. [[CrossRef](#)]
12. Cooke, D.R.; Bull, S.W.; Large, R.R.; McGoldrick, P.J. The Importance of Oxidized Brines for the Formation of Australian Proterozoic Stratiform Sediment-Hosted Pb-Zn (Sedex) Deposits. *Econ. Geol.* **2000**, *95*, 1–18. [[CrossRef](#)]
13. Mako, D.A.; Shanks, W.C. Stratiform Sulfide and Barite-Fluorite Mineralization of the Vulcan Prospect, Northwest Territories: Exhalation of Basinal Brines along a Faulted Continental Margin. *Can. J. Earth Sci.* **1984**, *21*, 78–91. [[CrossRef](#)]
14. Magnall, J.M.; Gleeson, S.A.; Blamey, N.J.F.; Paradis, S.; Luo, Y. The Thermal and Chemical Evolution of Hydrothermal Vent Fluids in Shale Hosted Massive Sulphide (SHMS) Systems from the MacMillan Pass District (Yukon, Canada). *Geochim. Cosmochim. Acta* **2016**, *193*, 251–273. [[CrossRef](#)]
15. Large, R.R.; Bull, S.W.; Cooke, D.R.; Mcgoldrick, P.J. A Genetic Model for the Hyc Deposit, Australia: Based on Regional Sedimentology, Geochemistry, and Sulfide-Sediment Relationships. *Econ. Geol.* **1998**, *93*, 1345–1368. [[CrossRef](#)]
16. Cameron, N.R.; Bennet, J.D.; Bridge, D.M.; Djunuddin, A.; Ghazali, S.A.; Harahap, H.; Jeffery, D.H.; Kartawa, W.; Keats, W.; Rock, N.M.S.; et al. *Geologic Map of the Tapaktuan Quadrangle, Sumatra (0519) Scale 1:250,000*; Geological Research and Development Centre: Bandung, Indonesian, 1982.
17. Rock, N.M.S.; Aldiss, D.T.; Aspden, J.A.; Clarke, M.C.G.; Djunuddin, A.; Kartawa, W.; Miswar; Thompson, S.J.; Whandoyo, R. *Geologic Map of the Lubuksikaping Quadrangle, Sumatra (0716) Scale 1:250,000*; Geological Research and Development Centre: Bandung, Indonesian, 1983.
18. Aldiss, D.T.; Whandoyo, R.; Ghazali, S.A. *Kusyono Geologic Map of the Sidikalang and (Part of) Sinabang Quadrangles, Sumatra Scale 1:250,000*; Geological Research and Development Centre: Bandung, Indonesian, 1983.
19. Pulunggono, A.; Cameron, N.R. Sumatran Microplates, Their Characteristics and Their Role in the Evolution of the Central and South Sumatra Basins. In Proceedings of the Proceedings of the 13th Annual Convention Indonesian Petroleum Association, Jakarta, Indonesia, 29–30 May 1984; pp. 121–143.
20. Barber, A.J.; Crow, M.J. Structure of Sumatra and Its Implications for the Tectonic Assembly of Southeast Asia and the Destruction of Paleotethys. *Isl. Arc.* **2009**, *18*, 3–20. [[CrossRef](#)]
21. Metcalfe, I. Conodont Faunas, Age and Correlation of the Alas Formation (Carboniferous), Sumatra. *Geol. Mag.* **1983**, *120*, 579–586. [[CrossRef](#)]
22. Barber, A.J.; Crow, M.J. Pre-tertiary stratigraphy. In *Sumatra: Geology, Resources and Tectonic Evolution*; Barber, A.J., Crow, M.J., Milsom, J.S., Eds.; The Geological Society: Bath, UK, 2005; pp. 24–53. [[CrossRef](#)]
23. Sato, T. Behaviours of Ore-Forming Solutions in Seawater. *Min. Geol.* **1972**, *22*, 31–42. [[CrossRef](#)]
24. Karpov, I.K.; Chudnenko, K.V.; Kulik, D.A. Modeling Chemical Mass-Transfer in Geochemical Processes: Thermodynamic Relations, Conditions of Equilibria and Numerical Algorithms. *Am. J. Sci.* **1997**, *297*, 767–806. [[CrossRef](#)]
25. Karpov, I.K.; Chudnenko, K.V.; Kulik, D.A.; Avchenko, O.V.; Bychinskii, V.A. Minimization of Gibbs Free Energy in Geochemical Systems by Convex Programming. *Geochem. Int.* **2001**, *39*, 1108–1119.
26. Wagner, T.; Kulik, D.A.; Hingerl, F.F.; Dmytrievava, S.V. Gem-Selektor Geochemical Modeling Package: TSolMod Library and Data Interface for Multicomponent Phase Models. *Can. Mineral.* **2012**, *50*, 1173–1195. [[CrossRef](#)]
27. Kulik, D.A.; Wagner, T.; Dmytrieva, S.V.; Kosakowski, G.; Hingerl, F.F.; Chudnenko, K.V.; Berner, U.R. GEM-Selektor Geochemical Modeling Package: Revised Algorithm and GEMS3K Numerical Kernel for Coupled Simulation Codes. *Comput. Geosci.* **2013**, *17*, 1–24. [[CrossRef](#)]
28. Huston, D.L. The Hydrothermal Environment. *AGSO J. Aust. Geol. Geophys.* **1998**, *17*, 15–30.
29. Boyce, A.J.; Barrie, C.D.; Samson, I.M.; Williams-Jones, A.E. *Current Perspectives on Zinc Deposits*; Archibald, S.M., Piercey, S.J., Eds.; Irish Association for Economic Geology: Dublin, Ireland, 2015.
30. The Chemical Composition of Seawater. Available online: <http://www.seafriends.org.nz/oceano/seawater.htm#composition> (accessed on 25 May 2021).
31. Wilkinson, J.J. Sediment-hosted zinc-lead mineralization: Processes and perspectives. In *Treatise on Geochemistry: Second Edition*; Holland, H.D., Turekian, K.K., Eds.; Elsevier Ltd.: Amsterdam, The Netherlands, 2014; Volume 13, pp. 219–249. [[CrossRef](#)]
32. Haas, J.L. Physical properties of the coexisting phases and thermochemical properties of the H₂O component in boiling NaCl solutions. In *U.S. Geological Survey Bulletin 1421-A*; U.S. Government Printing Office: Washington, DC, USA, 1976; p. 73.
33. Sawkins, F.J. Ore Genesis by Episodic De-Watering of Sedimentary Basins: Application to Giant Proterozoic Lead-Zinc Deposits. *Geology* **1984**, *12*, 451–454. [[CrossRef](#)]
34. Oliver, N.H.S.; McLellan, J.G.; Hobbs, B.E.; Cleverley, J.S.; Ord, A.; Feltrin, L. 100th Anniversary Special Paper: Numerical Models of Extensional Deformation, Heat Transfer, and Fluid Flow across Basement-Cover Interfaces during Basin-Related Mineralization. *Econ. Geol.* **2006**, *101*, 1–31. [[CrossRef](#)]
35. Gigon, J.; Deloule, E.; Mercadier, J.; Huston, D.L.; Richard, A.; Annesley, I.R.; Wygralak, A.S.; Skirrow, R.G.; Mernagh, T.P.; Masterman, K. Tracing Metal Sources for the Giant McArthur River Zn-Pb Deposit (Australia) Using Lead Isotopes. *Geology* **2020**, *48*, 478–482. [[CrossRef](#)]
36. Metcalfe, I. Tectonic Evolution of Sundaland. *Bull. Geol. Soc. Malaysia* **2017**, *63*, 27–60. [[CrossRef](#)]

37. Yardley, B.W.D. 100th Anniversary Special Paper: Metal Concentrations in Crustal Fluids and Their Relationship to Ore Formation. *Econ. Geol.* **2005**, *100*, 613–632. [[CrossRef](#)]
38. Tornos, F.; Heinrich, C.A. Shale Basins, Sulfur-Deficient Ore Brines and the Formation of Exhalative Base Metal Deposits. *Chem. Geol.* **2008**, *247*, 195–207. [[CrossRef](#)]
39. Ruaya, J.R.; Seward, T.M. The Stability of Chlorozinc(II) Complexes in Hydrothermal Solutions up to 350 °C. *Geochim. Cosmochim. Acta* **1986**, *50*, 651–661. [[CrossRef](#)]
40. Reed, M.H.; Palandri, J. Sulfide Mineral Precipitation from Hydrothermal Fluids. *Rev. Mineral. Geochem.* **2006**, *61*, 609–631. [[CrossRef](#)]
41. Seward, T.M.; Williams-Jones, A.E.; Migdisov, A.A. The Chemistry of Metal Transport and Deposition by Ore-Forming Hydrothermal Fluids. In *Treatise on Geochemistry: Second Edition*; Holland, H.D., Turekian, K.K., Eds.; Elsevier Ltd.: Amsterdam, The Netherlands, 2014; Volume 13, pp. 29–57. [[CrossRef](#)]
42. Seward, T.M.; Barnes, H.L. Metal transport in hydrothermal ore fluids. In *Geochemistry of Hydrothermal Ore Deposits*; Barnes, H.L., Ed.; Wiley Interscience: New York, NY, USA, 1997; pp. 435–486.